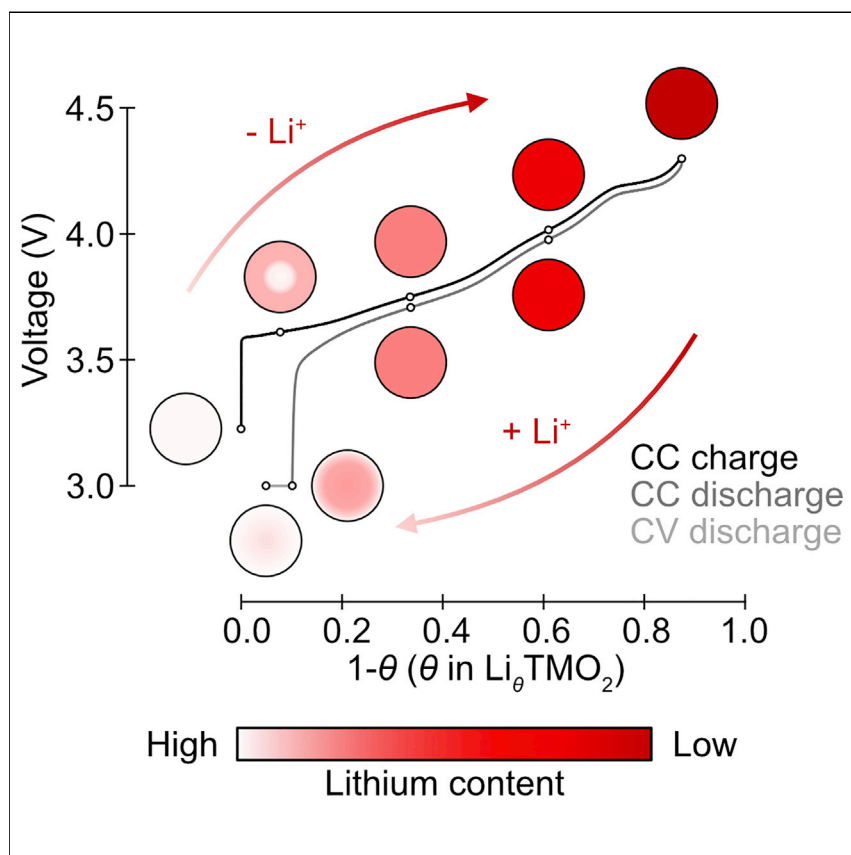**Article**

Operando visualization of kinetically induced lithium heterogeneities in single-particle layered Ni-rich cathodes

Optical scattering microscopy reveals lithium heterogeneity in NMC cathodes.

Chao Xu, Alice J. Merryweather, Shrinidhi S. Pandurangi, ..., Christoph Schnedermann, Akshay Rao, Clare P. Grey

cs2002@cam.ac.uk (C.S.)
ar525@cam.ac.uk (A.R.)
cpg27@cam.ac.uk (C.P.G.)

Highlights

Optical scattering microscopy reveals lithium heterogeneity in NMC single crystals

Charging and discharging in NMC kinetically limited by concentration-dependant diffusivity

Results explain ~10% capacity loss in NMC during the first cycle

Joule

Article

Operando visualization of kinetically induced lithium heterogeneities in single-particle layered Ni-rich cathodes

Chao Xu,[1,2,3,4,6] Alice J. Merryweather,[1,2,3,6] Shrinidhi S. Pandurangi,[3,5,6] Zhengyan Lun,[1,2,3] David S. Hall,[1,3] Vikram S. Deshpande,[3,5] Norman A. Fleck,[3,5] Christoph Schnedermann,[2,3,*] Akshay Rao,[2,3,*] and Clare P. Grey[1,3,7,*]

SUMMARY

Understanding how lithium-ion dynamics affect the (de)lithiation mechanisms of state-of-the-art nickel-rich layered oxide cathodes is crucial to improve electrochemical performance. Here, we directly observe two distinct kinetically induced lithium heterogeneities within single-crystal $LiNi_xMn_yCo_{(1-x-y)}O_2$ (NMC) particles using recently developed *operando* optical microscopy, challenging the notion that uniform (de)lithiation occurs within individual particles. Upon delithiation, a rapid increase in lithium diffusivity at the beginning of charge results in particles with lithium-poor peripheries and lithium-rich cores. The slow ion diffusion at near-full lithiation states—and slow charge transfer kinetics—also leads to heterogeneity at the end of discharge, with a lithium-rich surface preventing complete lithiation. Finite-element modeling confirms that concentration-dependent diffusivity is necessary to reproduce these phenomena. Our results demonstrate how kinetic limitations cause significant first-cycle capacity losses in Ni-rich cathodes.

INTRODUCTION

Layered Ni-rich NMCs ($LiNi_xMn_yCo_{(1-x-y)}O_2$, $x \geq 0.5$) and NCAs ($LiNi_xCo_yAl_{(1-x-y)}O_2$, $x \geq 0.5$) are widely used as cathode materials in high-energy-density lithium-ion batteries for electric vehicle applications.[1–4] Despite their cost and environmental benefits, these cathode materials suffer from long-term stability issues that limit their safety and lifetime, as well as typical irreversible capacity losses of >10% during the first cycle.[5–7] Significant world-wide effort is thus being devoted to understanding their underlying charging mechanisms to mitigate these shortcomings.[3,8,9] Previous studies have attributed the first-cycle capacity losses to kinetic limitations due to slow lithium diffusion at near-full lithiation states as a result of fewer lithium vacancies and decreased interlayer spacing.[10,11] X-ray diffraction (XRD)-based methods have furthermore revealed several "phase segregation" phenomena during the delithiation of Ni-based layered cathodes,[12–15] despite the fact that the (de)lithiation of such materials intrinsically follows a solid-solution mechanism.[12,16,17] Rather than a thermodynamic phase segregation, these observations suggest formation of kinetically controlled heterogeneities in lithium occupancy that occur over a sufficient domain size or length scale to result in discernible differences in the lattice constants and diffraction signals; however, a debate exists as to whether this heterogeneity is at the particle or electrode level.[14]

CONTEXT & SCALE

The mechanism by which lithium ions are stored in high-energy-density lithium-ion battery materials is typically assumed to be uniform across the individual active particles. Here, by using *operando* optical scattering microscopy and diffusive modeling, the authors directly image and track the buildup of kinetically induced lithium-ion heterogeneity within individual particles during battery operation in one of the most promising next-generation cathode materials based on nickel-rich manganese cobalt oxide (NMC).

The insights provided by this study do not only challenge long-held beliefs but also motivate new approaches to overcome critical capacity losses in high-performance materials, especially as society moves toward fast-charging regimes.

CellPress
OPEN ACCESS

Joule
Article

These proposed lithium heterogeneity phenomena are closely correlated with the electrochemical performance of the cathode material. However, our understanding of the operative mechanism by which the heterogeneity arises at the particle level is limited since many of these studies are based on ensemble characterization techniques, particularly *in situ* and *ex situ* XRD of bulk electrodes, where the measurements inherently cannot spatially resolve the heterogeneity at the relevant length scales.[12,13] Recent advances in synchrotron-based micro-spectroscopy techniques, such as scanning transmission X-ray microscopy (STXM) coupled with X-ray absorption spectroscopy,[14,18–20] are capable of providing chemical information at the nanometer scale. However, such techniques suffer from disadvantages including limited availability of beam time and potential beam damage.[21]

In this work, we directly track the lithium-ion dynamics in monolithic (also referred to as "single-crystal") Ni-rich NMC cathodes, with a particular focus on the transient lithium heterogeneities during lithium insertion and extraction, using a recently developed method—*operando* optical scattering microscopy.[22] Our results demonstrate a clear correlation between the optical intensity and local lithium content, and we identify kinetically induced lithium heterogeneities within individual active NMC particles. These heterogeneities are most prominent at the beginning of the charge and also appear at the end of discharge, originating from a sharp drop in the lithium-ion diffusion coefficient toward high lithium contents. We further explore the origins of these phenomena with finite-element modeling parameterized by a lithium concentration-dependent diffusion coefficient, derived from solid-state nuclear magnetic resonance (ssNMR) characterization. This combined approach enables us to determine the effects of the rate-limiting kinetic processes on the (de)lithiation of Ni-rich NMC cathodes and identify the conditions under which lithium heterogeneity occurs at the individual particle level. Via experiment and theory, we determine the origin of the first-cycle capacity loss in NMCs.

RESULTS

Operando optical scattering microscopy

During a typical *operando* measurement, an optically accessible electrochemical cell (Figure 1A) operates either under a constant-current (CC) or a constant-voltage (CV) bias and is simultaneously illuminated with a light-emitting diode (LED, central wavelength of 740 nm). The reflected and back-scattered light from the sample and the glass/electrolyte interface is collected and imaged onto a camera. Figure 1B shows an optical image of part of the NMC cathode with nominal stoichiometry $LiNi_{0.87}Mn_{0.05}Co_{0.08}O_2$, where the bright area corresponds to an individual ~2 μm NMC particle and the surrounding dark area represents the conductive carbon and binder matrix. The observed optical intensity is primarily determined by the local dielectric properties of the particle,[23–25] which are sensitive to the degree of lithiation.

The uniform optical intensity across the particle suggests that the top surface is smooth and flat, as further confirmed by a scanning electron microscope (SEM) image of the same particle (Figure 1C). Moreover, the flat surface is a strong indication that the observed surface is parallel to the NMC a/b basal plane (see the structure illustration in Figure 1D), which is further supported by the *operando* optical results discussed below.

XRD confirms the NMC is phase pure (space group $R\bar{3}m$) and has a low Li/Ni antisite mixing (~2%; diffraction pattern and Rietveld refinement results are shown in

[1]Yusuf Hamied Department of Chemistry, University of Cambridge, Cambridge, UK

[2]Cavendish Laboratory, University of Cambridge, Cambridge, UK

[3]The Faraday Institution, Quad One, Harwell Science and Innovation Campus, Didcot, UK

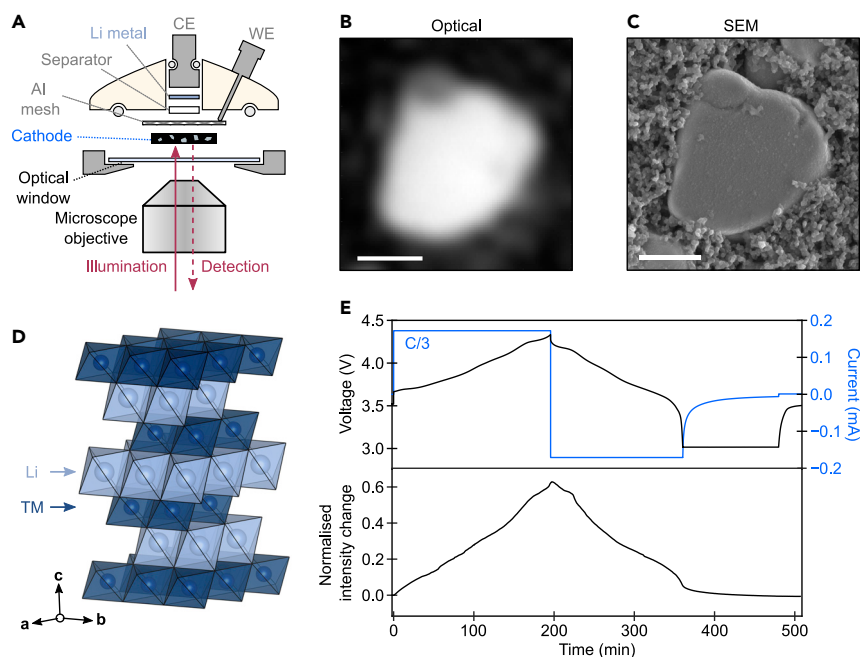[4]School of Physical Science and Technology, ShanghaiTech University, Shanghai, China

[5]Department of Engineering, University of Cambridge, Cambridge, UK

[6]These authors contributed equally

[7]Lead contact

*Correspondence: cs2002@cam.ac.uk (C.S.), ar525@cam.ac.uk (A.R.), cpg27@cam.ac.uk (C.P.G.)

https://doi.org/10.1016/j.joule.2022.09.008

Joule
Article

Figure 1. Monolithic NMC cathode and *operando* optical microscopy

(A) Schematic drawing of the key components of the electrochemical cell for optical microscopy. The cathode is a self-standing electrode composed of numerous NMC particles, carbon black and polytetrafluoroethylene (PTFE) binder. Aluminum mesh is used as a current collector (WE, working electrode; CE, counter electrode).

(B) Optical image of an active NMC particle in the electrochemical cell.

(C) SEM image of the same monolithic NMC particle shown in (B), obtained after the optical measurements.

(D) Schematic illustration of the crystal structure of the NMC cathode illustrating the alternating layers of LiO_6 and TMO_6 octahedra, where TM denotes transition metal.

(E) Voltage (black) and current (blue) profile (top panel) and the normalized optical intensity of the active particle shown in (B) (bottom panel) during one charge-discharge cycle (comprising a C/3 constant-current [CC] charge and discharge between 4.3 and 3 V, followed by a 2-h constant-voltage [CV] hold at 3 V. Three C/3 cycles were performed prior to this cycle, finishing with 2-h voltage holds at 3 V. The C-rate was calculated based on a practical capacity of 210 mA h g^{-1}, i.e., the current density for the C/3 rate is 70 mA g^{-1}. Scale bars, 1 μm.

Figure S5). Figure 1E shows a typical voltage (black line) and current (blue line) profile for a CC charge—CCCV discharge cycle at a C/3 rate (*n*C corresponds to a full charge or discharge in 1/*n* hours), with a 2-h voltage hold at 3 V at the end of discharge (full electrochemical cycling history is summarized in Figure S6). The CC charge and CC discharge capacities were 229.0 and 192.4 mA h g^{-1}, respectively, corresponding to a coulombic efficiency (CE) of 84.0%. The 2-h hold at 3 V provided an additional 16.4 mA h g^{-1}, increasing the CE to 91.2%. The extra discharge capacity obtained by applying a CV step at the end of CC discharge is a generic behavior for all layered Ni-rich cathodes.[5,13] Note that even with a CV hold, the CE of 91.2% is lower than that achieved in coin cells with an equivalent electrode and cycling procedure (typically >99% after the first cycle; see Figure S7), which we attribute to the performance limitations of the specialized *operando* cell.

On charge, the optical intensity of the active particle increases monotonically as lithium is de-intercalated from the NMC particle, reaching a maximum intensity ~62% higher than its initial value; the general trend is reversed on discharge/lithiation (bottom panel in Figure 1E; Video S1). This clearly shows that the dielectric

Joule
Article
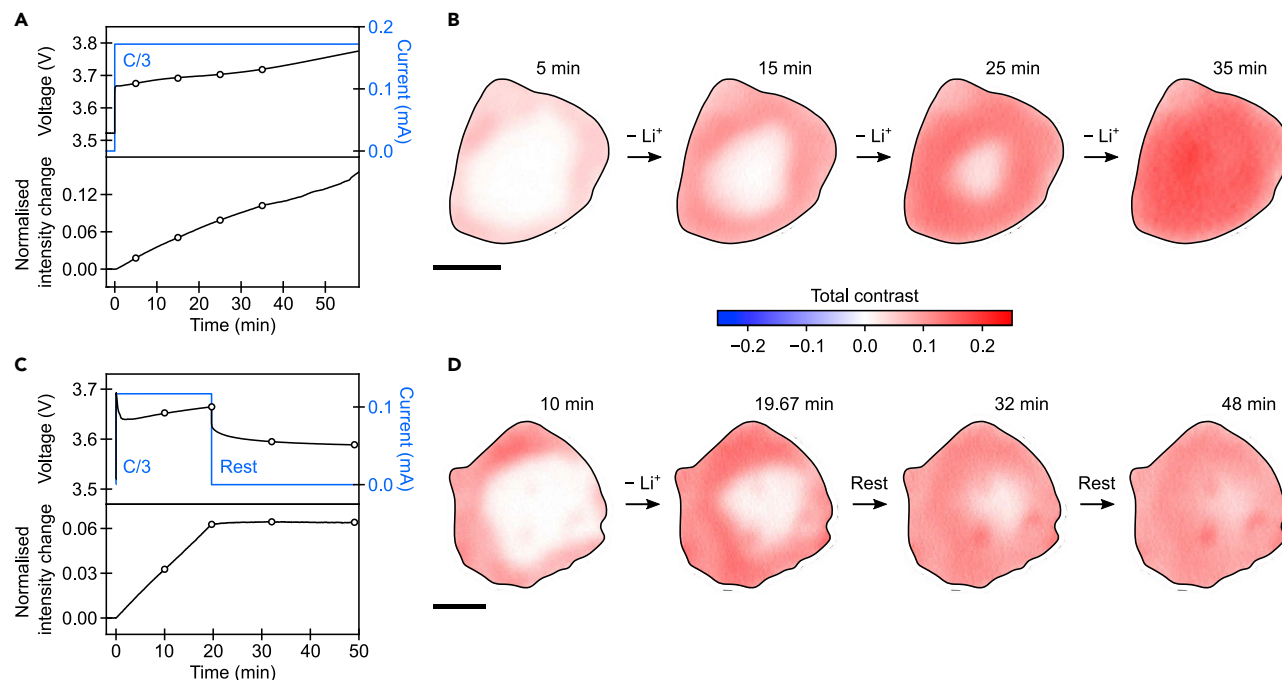
Figure 2. Lithium heterogeneity in single-particle NMC at the beginning of charge
(A) Voltage and current profiles during the first 1 h of charge at C/3 (top panel) and the normalized intensity changes, obtained by integrating over the whole active particle shown in (B) (bottom panel).
(B) Normalized differential images of the active particle during the initial charging, for the time points indicated by black circles in (A). The total contrast is shown, which represents the fractional intensity change between the current frame and the first frame of the cycle (i.e., with no current applied). The color scale is centered at zero (white), with positive values indicating an overall intensity increase (red), and negative values indicating a decrease (blue).
(C) Voltage and current profiles during the first 20 min of charge at C/3 followed by a rest period (top panel), and the normalized intensity changes of a second active particle (bottom panel).
(D) Normalized differential images of the active NMC particle during the charge-rest experiment. Scale bars, 1 μm.

properties of the NMC cathode are strongly dependent on its lithium content. Moreover, the monotonic nature of the intensity change means that intensity can be used as a qualitative proxy for the single-particle state-of-charge (SoC)/lithium content: a higher intensity corresponds to a lower lithium content. A more detailed analysis of the relationship between the optical intensity and lithium content is given in Figure S8, and the smaller changes seen above 4.1 V are shown in Figure S9.

Lithium heterogeneity at the beginning of charge

We now investigate spatially resolved delithiation and lithiation processes in single-particle NMCs. Figure 2A shows the voltage profile and intensity change during the first hour of the C/3 charge, and differential images (see experimental procedures) with respect to the beginning of the cycle at 5, 15, 25, and 35 min are shown in Figure 2B. After 5 min of delithiation at C/3, the periphery of the particle started to show a positive contrast, the higher intensity being ascribed to local NMC domains with lower lithium content (higher intensity is indicative of lower lithium content; Figure 1D). The core remains fully lithiated and a distinct lithium concentration heterogeneity inside this individual NMC particle is formed. On further charging, this periphery continued to advance toward the center of the particle, further increasing in positive contrast, while the core lagged noticeably behind (15 and 25 min, Figure 2B). After 35 min, the total contrast had become reasonably uniform across the whole particle (Video S2). We have observed this phenomenon in more than 50 different particles from seven different electrodes, confirming its reproducibility

Joule
Article

(see Figure S10). Further work on a larger set of particles is required to explore further heterogeneity effects and identify other correlations between, for example, size and shape and heterogeneity/diffusivity.

This apparent "core-shell" structure cannot be of thermodynamic origin since the (de)lithiation of Ni-rich materials is widely acknowledged to be a solid-solution process. This is in contrast to the closely related material $LiCoO_2$, which exhibits a thermodynamic two-phase region at the beginning of the charge caused by an insulator-to-metal transition, absent in NMC.[26–28] A charge-rest experiment was then performed to confirm the kinetic origin of the "core-shell" structure observed here (Figure 2C). During the ~20-min charge period, lithium heterogeneity began to develop in the particle as described above (Figure 2D). After stopping the current, however, the intensity heterogeneity across the particle gradually disappeared, and a uniform distribution was achieved by the end of the rest period (Figure 2D)—this is consistent with a kinetically driven intra-particle heterogeneity where the equilibrium state exhibits a uniform lithium distribution.

In addition to the intra-particle heterogeneity discussed above, some inter-particle reaction heterogeneity was also observed at the beginning of the charge at a higher rate of 2C (Figure S11). We ascribe this observation to differences in wiring and tortuosity of pathways for lithium transport through the bulk electrode to the NMC particles since the particles that are imaged are located the furthest from the separator (see Figure 1A and Video S3). Further studies are currently underway to quantify these effects.

Finite-element simulations and rate dependence

Guided by the experimental results, we developed a finite-element model to assist our understanding of the lithium heterogeneity observed at the beginning of the charge. Our model assumes a constant lithium flux in/out of a particle—the particle has the same cross-sectional shape as one of the particles that were examined experimentally (Figure 3A), with diffusion only occurring parallel to the basal plane of the particle. To calculate the self-diffusion coefficient, D_{Li}, of lithium inside the NMC lattice, we measured the lithium hop rate ν using solid-state NMR as a function of SoC and inferred D_{Li} from ν (see supplemental information section "ssNMR and self-diffusion coefficients").

Note that the inferred magnitude of ν depends strongly on assumptions made as part of the NMR data analysis as discussed below (supplemental information section "modeling"). Therefore, instead of directly using the value of D_{Li} inferred from the NMR hop rate data, we scaled D_{Li} by a constant factor S to obtain an effective diffusion coefficient $D_{Li}^{eff} \equiv D_{Li}/S$ while not changing the functional form of the dependence of D_{Li} on SoC. The scaling factor S was obtained by seeking for agreement between predictions of occupancy and measurements of the temporal variation of the total contrast within the NMC particle. Specifically, we assumed a linear relation between optical intensity and Li occupancy and obtained S by minimizing the root-mean-square error between the temporal intensity measurements at the center of the particle and the corresponding occupancy predictions at a charging rate of C/3. This analysis suggests $S = 3.5$ (see supplemental information and Figure S2) such that $D_{Li}^{eff} \sim 10^{-14} cm^2 \, s^{-1}$ near-full lithiation. Regardless of the value of S, D_{Li}^{eff} increases by almost two orders of magnitude upon removal of 40% of the lithium (Figure 3B). Upon adopting this calibrated value of D_{Li}^{eff}, the model captures the spatio-temporal evolution of Li occupancy within the NMC particle including the
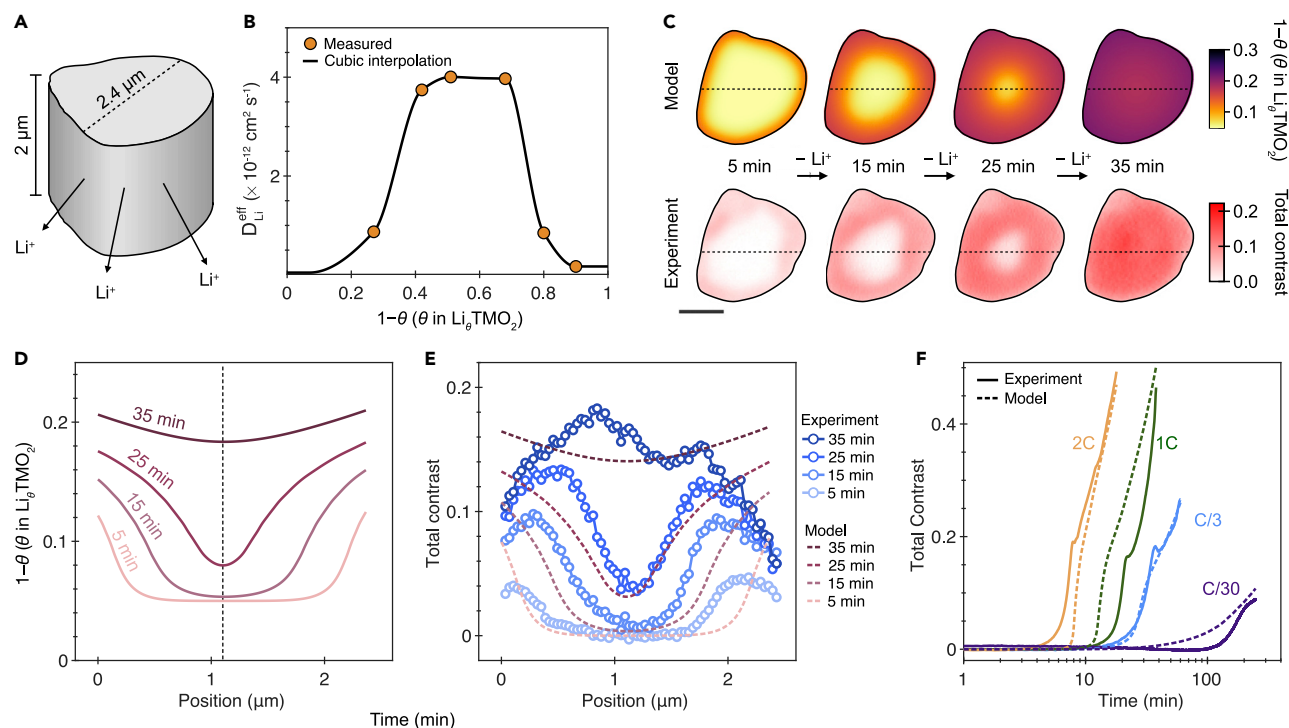
Figure 3. Comparing modeling and experiments

(A) Sketch of the particle used in the modeling.

(B) The effective lithium diffusion coefficient $D_{Li}^{eff} \equiv D_{Li}/S$ as a function of lithium content ($S = 3.5$).

(C) Comparison of simulation and experimental imaging results, both conducted at a delithiation rate of C/3. The predicted degree of delithiation ($1 - \theta$) on the basal plane of the particle at various times during the charge.

(D and E) Evolution of (D) the degree of delithiation in the simulation and (E) the total contrast in the optical images along the horizontal dotted line marked in (C). In (E), we include the corresponding predictions (shown with dashed curves) of the total contrast.

(F) Evolution of measurements and predictions of total contrast at the center of the particle (shown by the vertical dashed lines in D).

development of sharp concentration gradients during delithiation at C/3 (Figures 3C–3E). These spatial heterogeneities occur over a wide range of charging rates, and the model reproduces these observations for charging rates ranging from C/30 to 2C (Figures S12 and S13).

The lithium heterogeneity during charging can be succinctly illustrated by retrieving the lithium content at the center of the particle (Figure 3F). Again, the model is in good agreement with experimental results and clearly shows that the delithiation of the particle center lags noticeably behind the surface at the start of the CC charge at all charging rates, indicating that the delithiation front takes significant time to reach the center. Our model also indicates that the intra-particle heterogeneity is strongly dependent on the particle size, i.e., smaller particles show less pronounced heterogeneity (Figures S14 and S15), which is in good agreement with the experiment (Figure S16; Video S4). We note that our modeling revealed that some spatial lithium-ion heterogeneity can also arise when the ion diffusivity is assumed to be constant but small in magnitude and below 5×10^{-14} cm^2 s^{-1}, see Figure S17D. However, the temporal evolution of the ion concentration assuming a constant diffusivity fails to capture the delayed response of the particle center followed by a quick delithiation (Figure S17) as seen in the experimentally observed intensity measurements (Figure 3F). Taken together, these results strongly support our hypothesis that the observed heterogeneous delithiation is consistent with a strong sensitivity of diffusivity to lithium content at the beginning of the charge.

CellPress
OPEN ACCESS
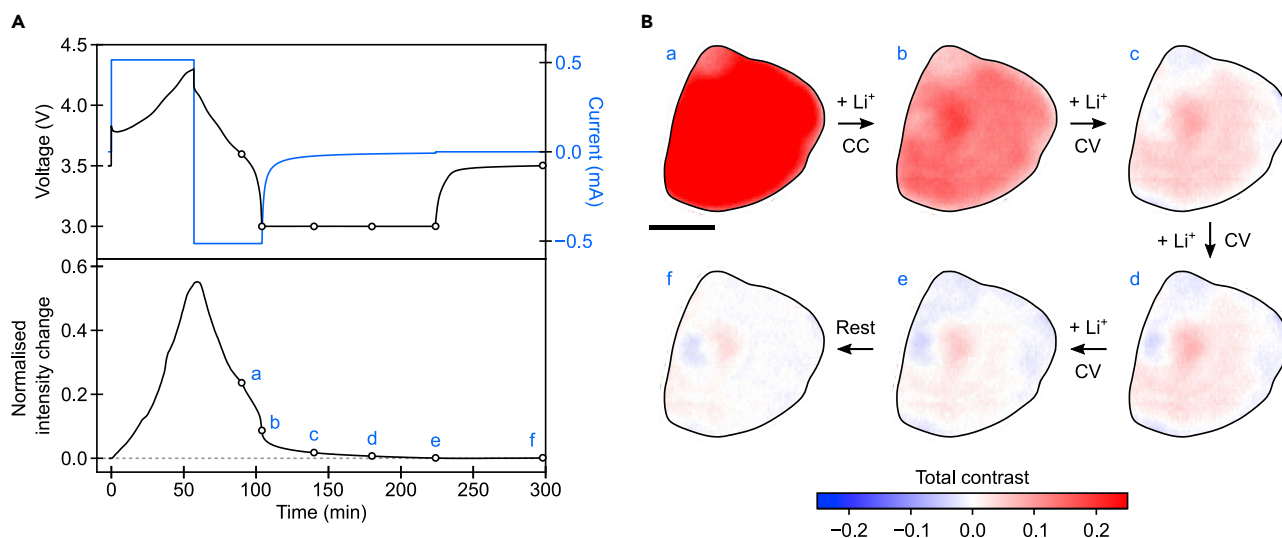
Figure 4. Lithium heterogeneity at the end of discharge

(A) Voltage and current profile (top panel) and normalized intensity changes of the active particle during a 1C rate CC charge and CCCV discharge cycle. CV was performed at 3 V for 2 h. The dashed gray line (bottom panel) is a guide for the eye, representing 0 intensity change. The initial lithium content is estimated to be ~97% based on the open circuit voltage (OCV, ~3.5 V versus Li/Li$^+$). Note that this near-full lithiation state was achieved by applying a 2-h voltage hold at 3 V after the end of CC discharge in the previous cycle.

(B) Differential images of an NMC active particle during the discharge, at the times indicated by black circles in (A) (where a, b, c, d, e, and f are at 90, 104, 140, 180, 224, and 298 min, respectively). Scale bars, 1 μm. The current at the end of the CV period was −7.59 μA (equivalent to ~C/200; a negative sign denotes discharging current).

Lithium heterogeneity at the end of discharge

We next explored in more detail how these dynamic lithium heterogeneities influence the first-cycle capacity loss in layered Ni-rich materials. During CC cycling at 1C (Figure 4A), the normalized intensity of the particle followed the same trends as seen above. Importantly, however, at the end of discharge, the particle intensity was 8% higher than its initial value, indicating incomplete reinsertion of lithium, in line with the voltage-capacity profile (Figure S18). During a subsequent 2-h CV hold at 3 V, an extra capacity of ~24 mA h g^{-1} could be extracted (increasing the CE from 82.3% to 94.3%), and the mean intensity reached its initial value.

Examining the spatial intensity variations across the particle shows that the intensity of the active particle remained uniform for the first 30 min of the 1C discharge (a in Figure 4B). At the end of the CC discharge (104 min, b in Figure 4B), the vast majority of the particle still exhibited a lower lithium content (positive total contrast, red) compared with the beginning of the charge. Yet, around a narrow periphery of the particle, the total contrast was close to zero (Figure S18), indicating that the particle has a lithium-rich periphery (with the lithium content approaching that of the particle before charging) and a more lithium-deficient core. The fact that the core remains lithium deficient can be explained by the drastically reduced lithium diffusion coefficient at near-full lithiation states (Figure S19).[11,14] For occupancy of $(1 - \theta) < 0.2$, the drop in diffusivity produces a significant concentration gradient across the particle, which is more pronounced at faster-charging rates (Figure S19).

With the additional CV step, the particle was re-lithiated further as indicated by the continued decrease in total contrast (c, d, and e in Figure 4B). In particular, a large fraction of the particle returned to the initial intensity (~0 total contrast, white). At the end of the CV step (e in Figure 4B), the variation in the contrast (hence the lithium

CellPress
OPEN ACCESS

Joule
Article
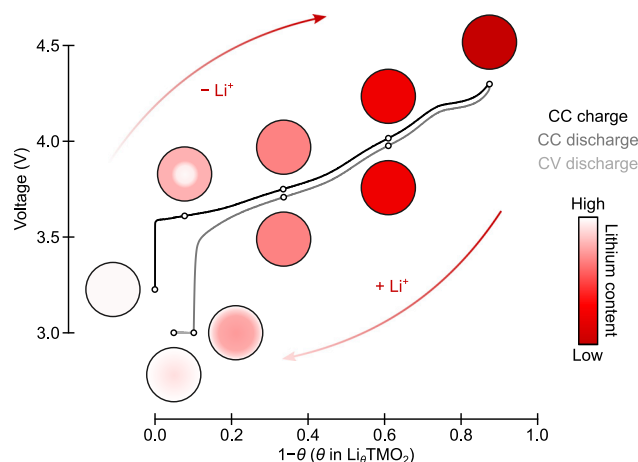
Figure 5. Summary of the lithium-ion distribution within the single active particle at various lithium contents

The circles show schematic representations of single-particle Ni-rich materials at various SoCs. The voltage profile is illustrative of the single-crystal NMC material used in this work and was obtained in a half-cell cycled with a CC charge and CC discharge (C/20 rate) and a discharge CV hold at 3 V (for 24 h).

content) across the particle becomes very small, and further equilibration is seen after the open circuit voltage (OCV) rest (f in Figure 4B). These results confirm that the capacity loss induced by the kinetic limitations mentioned above can be, to a large extent, recovered by a slow lithiation step. Note that even with a very long voltage hold at the end of discharge, the first-cycle CE still does not reach 100%, as demonstrated here (Figure 5) and in other studies in the literature.[5,13,29] The CE of coin cells is, however, significantly higher, and the poorer CE in the optical experiments is attributed to the unconventional cell setup (see Figures S6 and S7). The remaining first-cycle loss is attributed to electrolyte degradation at high voltages and mechanisms associated with a loss of active material due to, for instance, transition metal dissolution[30–32] and surface reconstruction.[33–35] Consistent with this, the CE increases as the rate increases approaching 98% at 2C (see Figure S6), the electrodes spending less time at higher voltages. Given the extremely low diffusivity of the fully lithiated material with no Li vacancies, it is also possible that not all of the particles in the whole electrode are fully lithiated even after the long hold.

DISCUSSION

Lithium heterogeneities during delithiation and lithiation

When delithiating the layered cathodes from full (and near-full) lithiation states, a noticeable lithium heterogeneity is seen with a lithium-rich core and a lithium-poor periphery (summarized in Figure 5). The SoC range during which this heterogeneity is present is dependent on the initial state of charge as well as the charging rate. This lithium heterogeneity arises from the low lithium diffusivity at near-full lithiation, which is insufficient to support a high lithium-ion flux uniformly throughout the particle. Instead, as the lithium is extracted from the periphery of the particle, the periphery develops a higher lithium diffusivity due to its lower lithium occupancy, accelerating the rate of lithium-ion extraction from the lithium-poor periphery domains further. Simultaneously, the boundary between the lithium-rich and lithium-poor domains propagates toward the center of the particle as the charging progresses, until the particle becomes uniform in lithium content, and no obvious heterogeneity occurs during the rest of the charging.

Joule
Article

CellPress
OPEN ACCESS

During CV discharge, lithium insertion occurs predominantly uniformly throughout the particle, except at the very end where a narrow periphery becomes notably lithium-rich compared with the core. This results from two kinetic limitations, slow lithium diffusion—seen by ssNMR measurements—and slow charge transfer kinetics (see potentiostatic intermittent titration results in Figure S20), both of which lead to a substantial increase in the over-potential and hence a steep decrease in the cell voltage during CC discharge. As a result, the cell quickly reaches the cut-off voltage with the core of the NMC particles in a lithium-deficient state and therefore causes a capacity loss. Such kinetic limitations can be largely overcome by a much slower lithiation process, for instance, by inserting a CV hold at 3 V versus Li/Li$^+$ in the present case. Although the degree of heterogeneity at the end of discharge is much less significant than that seen at the beginning of the charge, it is nonetheless capable of resulting in a loss in capacity of as much as 10% when using standard CC cycling regimes.

Lithium heterogeneity in related NCA materials at the beginning of the first charge was proposed recently by Grenier et al.,[13] in the SoC range of $0.96 > \theta > 0.74$ on the basis of *operando* synchrotron powder XRD. Here, the XRD pattern was modeled with two different phases, with the difference in lithium content between the lithium-poor and the lithium-rich phase gradually increasing from 0.09 at $\theta = 0.96$ to 0.18 at $\theta = 0.74$—such lithium heterogeneity was ascribed to be intra-particle. XRD, however, is a bulk technique and provides no spatially resolved information. Conversely, Park et al. recently suggested, on the basis of *ex situ* X-ray absorption microscopy experiments, that this heterogeneity occurs between, rather than within, particles.[14] They proposed an intrinsic mechanism for the apparent phase separation observed during the delithiation of NMC, termed "electro-autocatalysis," which describes the increase in the interfacial exchange current density as lithium content decreases.[14]

Our work expands on these studies, directly demonstrating that both proposed mechanisms will be at play under operating conditions. Critically, the intra-particle heterogeneity observed in our work cannot be captured by *ex situ* experiments (see Figure 2D). We further note that non-uniform lithiation during the CC and CV discharge has not been previously seen by XRD,[13] presumably because it represented a very small fraction of the bulk, highlighting the unique capability of our optical imaging technique to capture the transient and small heterogeneities in battery materials.

A scaling factor of 3.5 was needed to reconcile the NMR-derived diffusivities and those predicted on the basis of the finite-element modeling. This is (as discussed in the supplemental information) ascribed to the errors implicit in the extraction of NMR hop rates in the NMR experiment, where we used the NMR-derived maximum hopping rate and did not include the distributions of correlation times seen experimentally, nor the nature of the hops of the Li$^+$ ions in between the NMC layers. The diffusivities extracted from the simulations represent the effective diffusivities on a 2D lattice during cycling. Future experiments and simulations will explore how these vary from particle to particle and as a function of transition metal content in the NMC material.

Practical implications

The lithium heterogeneity at the beginning of the charge will generate a noticeable difference in lattice constants between the lithium-rich and lithium-poor domains. At fast C-rates, for instance, 1C and 2C, the SoC difference between the periphery and the core can be as large as 20%–30% within a narrow length scale based on our modeling (Figure S13). This large concentration gradient will lead to internal stress/strain within individual particles, which may further result in mechanical degradation such as particle fracturing, especially for larger particle sizes. Moreover, the first-cycle CE loss is of

particular importance since it reduces the energy density of practical cells: although graphite anode performances have been continuously improved with the first-cycle CEs now approaching 96%,[36] that of the Ni-rich materials is limited to ~90%. Therefore, increasing the first-cycle efficiency of the cathode can lead to a direct increase in the reversible energy density at the cell level. Such an increase will be more evident for the next generation of high-energy-density batteries consisting of a Ni-rich cathode and a lithium metal anode. Our results show that the key to improving performance lies in increasing the lithium mobility and charge transfer kinetics at near-full lithiation states. Although current literature is yet inconclusive as to what may be the most effective approaches to improve the first-cycle CE, certain coating materials—for instance, Nb-containing compounds[37]—have been shown to be promising.

Concluding remarks

In this work, we employed *operando* optical microscopy to track the lithium-ion dynamics in single-particle layered Ni-rich NMC, with a particular focus on understanding the transient lithium heterogeneities at the single-particle scale. The observed optical intensity revealed a substantial increase upon delithiation (charge) and a decrease upon lithiation (discharge), indicating that the optical intensity can be used as a qualitative probe for the local lithium content.

The spatially resolved intensity changes showed clear lithium heterogeneity at the beginning of the charge, exhibiting particles with a lithium-poor periphery and lithium-rich core. This intra-particle heterogeneity persisted across a wide range of C-rates, from C/30 to 2C. By developing a finite-element model, we demonstrated that this phenomenon is due to a kinetic diffusion-driven mechanism, caused by low lithium diffusivity at near-full lithiation states, which increases dramatically on delithiation. Combining the optical results with ssNMR and modeling, we extracted accurate values for the concentration-dependent lithium-ion diffusion coefficient of the Ni-rich NMC cathode material under study.

We further showed that when approaching high lithiation states on discharge, the NMC particle surface gradually becomes saturated by lithium due to the decreased lithium diffusivity at high lithiation states. Coupled with slow charge transfer kinetics, this is one of the main reasons for the first-cycle Coulombic inefficiency of layered Ni-rich materials. These results pave the way toward a better understanding of possible improvements in current state-of-the-art NMC materials and more broadly highlight the importance of understanding nanoscale dynamic changes in battery materials during their operation.

EXPERIMENTAL PROCEDURES

Resource availability

Lead contact

Further information and requests for resources should be directed to and will be fulfilled by the lead contact, Clare P. Grey (cpg27@cam.ac.uk).

Materials availability

This study did not generate new unique reagents.

Data and code availability

The data supporting the findings of this study are available within the main text and the supplemental information. More detailed data and the code for simulation can be made available upon request to the corresponding author.

Full experimental procedures are provided in the supplemental information.

Joule
Article

AUTHOR CONTRIBUTIONS

C.P.G., A.R., and C.S. conceived the idea of this work. C.X., A.J.M., Z.L., and C.S. performed the *operando* optical microscopy experiments. C.X. analyzed the optical microscopy data with support from A.J.M., Z.L., and C.S. C.X. performed electrochemical characterizations and SEM and analyzed the data. Z.L. performed XRD. C.X. performed the Rietveld Refinement. D.S.H. performed ssNMR measurements and analyzed data. S.S.P. developed the model and carried out finite-element simulations under the guidance of N.A.F. and V.S.D. All authors discussed the results and contributed to the manuscript writing.

DECLARATION OF INTERESTS

A.J.M., C.S., A.R., and C.P.G. are founders of Illumion, Ltd.

INCLUSION AND DIVERSITY

We support the inclusive, diverse, and equitable conduct of research.

REFERENCES

1. Blomgren, G.E. (2017). The development and future of lithium ion batteries. J. Electrochem. Soc. *164*, A5019–A5025. https://doi.org/10.1149/2.0251701jes.

2. Li, W., Erickson, E.M., and Manthiram, A. (2020). High-nickel layered oxide cathodes for lithium-based automotive batteries. Nat. Energy *5*, 26–34. https://doi.org/10.1038/s41560-019-0513-0.

3. Choi, J.U., Voronina, N., Sun, Y.-K., and Myung, S.-T. (2020). Recent progress and perspective of advanced high-energy Co-Less Ni-Rich cathodes for Li-ion batteries: yesterday, today,

and tomorrow. Adv. Energy Mater. *10*, 2002027. https://doi.org/10.1002/aenm.202002027.

4. Grey, C.P., and Hall, D.S. (2020). Prospects for lithium-ion batteries and beyond—a 2030 vision. Nat. Commun. *11*, 6279. https://doi.org/10.1038/s41467-020-19991-4.

5. Zhou, H., Xin, F., Pei, B., and Whittingham, M.S. (2019). What limits the capacity of layered oxide cathodes in lithium batteries? ACS Energy Lett. *4*, 1902–1906. https://doi.org/10.1021/acsenergylett.9b01236.

6. Xie, Q., Li, W., and Manthiram, A. (2019). A Mg-doped high-nickel layered oxide cathode enabling safer, high-energy-density Li-ion batteries. Chem. Mater. *31*, 938–946. https://doi.org/10.1021/acs.chemmater.8b03900.

7. Kim, U.-H., Park, G.-T., Son, B.-K., Nam, G.W., Liu, J., Kuo, L.-Y., Kaghazchi, P., Yoon, C.S., and Sun, Y.-K. (2020). Heuristic solution for achieving long-term cycle stability for Ni-rich layered cathodes at full depth of discharge. Nat. Energy *5*, 860–869. https://doi.org/10.1038/s41560-020-00693-6.

CellPress
OPEN ACCESS

Joule
Article

8. Li, W., Liu, X., Celio, H., Smith, P., Dolocan, A., Chi, M., and Manthiram, A. (2018). Mn versus Al in Layered Oxide Cathodes in lithium-Ion Batteries: A Comprehensive Evaluation on Long-Term Cyclability. Adv. Energy Mater. 8, 1703154. https://doi.org/10.1002/aenm.201703154.

9. Ryu, H.-H., Namkoong, B., Kim, J.-H., Belharouak, I., Yoon, C.S., and Sun, Y.-K. (2021). Capacity fading mechanisms in Ni-Rich Single-Crystal NCM cathodes. ACS Energy Lett. 6, 2726–2734. https://doi.org/10.1021/acsenergylett.1c01089.

10. Märker, K., Xu, C., and Grey, C.P. (2020). Operando NMR of NMC811/graphite lithium-ion batteries: structure, dynamics, and lithium metal deposition. J. Am. Chem. Soc. 142, 17447–17456. https://doi.org/10.1021/jacs.0c06727.

11. Ge, M., Wi, S., Liu, X., Bai, J., Ehrlich, S., Lu, D., Lee, W.K., Chen, Z., and Wang, F. (2021). Kinetic limitations in single-crystal high-nickel cathodes. Angew. Chem. Int. Ed. Engl. 60, 17350–17355. https://doi.org/10.1002/anie.202012773.

12. Grenier, A., Liu, H., Wiaderek, K.M., Lebens-Higgins, Z.W., Borkiewicz, O.J., Piper, L.F.J., Chupas, P.J., and Chapman, K.W. (2017). Reaction heterogeneity in $LiNi_{0.8}Co_{0.15}Al_{0.05}O_2$ induced by surface layer. Chem. Mater. 29, 7345–7352. https://doi.org/10.1021/acs.chemmater.7b02236.

13. Grenier, A., Reeves, P.J., Liu, H., Seymour, I.D., Märker, K., Wiaderek, K.M., Chupas, P.J., Grey, C.P., and Chapman, K.W. (2020). Intrinsic kinetic limitations in substituted lithium-layered transition-metal oxide electrodes. J. Am. Chem. Soc. 142, 7001–7011. https://doi.org/10.1021/jacs.9b13551.

14. Park, J., Zhao, H., Kang, S.D., Lim, K., Chen, C.C., Yu, Y.S., Braatz, R.D., Shapiro, D.A., Hong, J., Toney, M.F., et al. (2021). Fictitious phase separation in Li layered oxides driven by electro-autocatalysis. Nat. Mater. 20, 991–999. https://doi.org/10.1038/s41563-021-00936-1.

15. Xu, C., Märker, K., Lee, J., Mahadevegowda, A., Reeves, P.J., Day, S.J., Groh, M.F., Emge, S.P., Ducati, C., Layla Mehdi, B., et al. (2021). Bulk fatigue induced by surface reconstruction in layered Ni-rich cathodes for Li-ion batteries. Nat. Mater. 20, 84–92. https://doi.org/10.1038/s41563-020-0767-8.

16. Märker, K., Reeves, P.J., Xu, C., Griffith, K.J., and Grey, C.P. (2019). Evolution of structure and lithium dynamics in $LiNi_{0.8}Mn_{0.1}Co_{0.1}O_2$ (NMC811) cathodes during electrochemical cycling. Chem. Mater. 31, 2545–2554. https://doi.org/10.1021/acs.chemmater.9b00140.

17. Xu, C., Reeves, P.J., Jacquet, Q., and Grey, C.P. (2021). Phase behavior during electrochemical cycling of Ni-Rich cathode materials for Li-ion

batteries. Adv. Energy Mater. 11, 2003404. https://doi.org/10.1002/aenm.202003404.

18. Tian, C., Xu, Y., Nordlund, D., Lin, F., Liu, J., Sun, Z., Liu, Y., and Doeff, M. (2018). Charge heterogeneity and surface chemistry in polycrystalline cathode materials. Joule 2, 464–477. https://doi.org/10.1016/j.joule.2017.12.008.

19. Cao, C., Toney, M.F., Sham, T.-K., Harder, R., Shearing, P.R., Xiao, X., and Wang, J. (2020). Emerging X-ray imaging technologies for energy materials. Mater. Today 34, 132–147. https://doi.org/10.1016/j.mattod.2019.08.011.

20. Lu, J., Wu, T., and Amine, K. (2017). State-of-the-art characterization techniques for advanced lithium-ion batteries. Nat. Energy 2, 17011. https://doi.org/10.1038/nenergy.2017.11.

21. Martens, I., Melo, L.G.A., Wilkinson, D.P., Bizzotto, D., and Hitchcock, A.P. (2019). Characterization of X-ray damage to perfluorosulfonic acid using correlative microscopy. J. Phys. Chem. C 123, 16023–16033. https://doi.org/10.1021/acs.jpcc.9b03924.

22. Merryweather, A.J., Schnedermann, C., Jacquet, Q., Grey, C.P., and Rao, A. (2021). Operando optical tracking of single-particle ion dynamics in batteries. Nature 594, 522–528. https://doi.org/10.1038/s41586-021-03584-2.

23. Ortega-Arroyo, J., and Kukura, P. (2012). Interferometric scattering microscopy (iSCAT): new frontiers in ultrafast and ultrasensitive optical microscopy. Phys. Chem. Chem. Phys. 14, 15625–15636. https://doi.org/10.1039/c2cp41013c.

24. Piliarik, M., and Sandoghdar, V. (2014). Direct optical sensing of single unlabelled proteins and super-resolution imaging of their binding sites. Nat. Commun. 5, 4495. https://doi.org/10.1038/ncomms5495.

25. Gholami Mahmoodabadi, R., Taylor, R.W., Kaller, M., Spindler, S., Mazaheri, M., Kasaian, K., and Sandoghdar, V. (2020). Point spread function in interferometric scattering microscopy (iSCAT). Part I: aberrations in defocusing and axial localization. Opt. Express 28, 25969–25988. https://doi.org/10.1364/OE.401374.

26. Marianetti, C.A., Kotliar, G., and Ceder, G. (2004). A first-order Mott transition in Li_xCoO_2. Nat. Mater. 3, 627–631. https://doi.org/10.1038/nmat1178.

27. Ménétrier, M., Carlier, D., Blangero, M., and Delmas, C. (2008). On "really" stoichiometric $LiCoO_2$. Electrochem. Solid State Lett. 11, A179. https://doi.org/10.1149/1.2968925.

28. Ménétrier, M., Saadoune, I., Levasseur, S., and Delmas, C. (1999). The insulator-metal transition upon lithium deintercalation from

$LiCoO_2$: electronic properties and ^7Li NMR study. J. Mater. Chem. 9, 1135–1140. https://doi.org/10.1039/A900016J.

29. Seidlmayer, S., Buchberger, I., Reiner, M., Gigl, T., Gilles, R., Gasteiger, H.A., and Hugenschmidt, C. (2016). First-cycle defect evolution of $Li_{1-x}Ni_{1/3}Mn_{1/3}Co_{1/3}O_2$ lithium ion battery electrodes investigated by positron annihilation spectroscopy. J. Power Sources 336, 224–230. https://doi.org/10.1016/j.jpowsour.2016.10.050.

30. Wandt, J., Freiberg, A., Thomas, R., Gorlin, Y., Siebel, A., Jung, R., Gasteiger, H.A., and Tromp, M. (2016). Transition metal dissolution and deposition in Li-ion batteries investigated by operando X-ray absorption spectroscopy. J. Mater. Chem. A 4, 18300–18305. https://doi.org/10.1039/C6TA08865A.

31. Zhan, C., Wu, T., Lu, J., and Amine, K. (2018). Dissolution, migration, and deposition of transition metal ions in Li-ion batteries exemplified by Mn-based cathodes – a critical review. Energy Environ. Sci. 11, 243–257. https://doi.org/10.1039/C7EE03122J.

32. Ruff, Z., Xu, C., and Grey, C.P. (2021). Transition metal dissolution and degradation in NMC811-graphite electrochemical cells. J. Electrochem. Soc. 168, 060518. https://doi.org/10.1149/1945-7111/ac0359.

33. Lin, F., Markus, I.M., Nordlund, D., Weng, T.-C., Asta, M.D., Xin, H.L., and Doeff, M.M. (2014). Surface reconstruction and chemical evolution of stoichiometric layered cathode materials for lithium-ion batteries. Nat. Commun. 5, 3529. https://doi.org/10.1038/ncomms4529.

34. Streich, D., Erk, C., Guéguen, A., Müller, P., Chesneau, F.-F., and Berg, E.J. (2017). Operando monitoring of early Ni-mediated surface reconstruction in layered lithiated Ni–Co–Mn oxides. J. Phys. Chem. C 121, 13481–13486. https://doi.org/10.1021/acs.jpcc.7b02303.

35. Li, L., Self, E.C., Darbar, D., Zou, L., Bhattacharya, I., Wang, D., Nanda, J., and Wang, C. (2020). Hidden subsurface reconstruction and its atomic origins in layered oxide cathodes. Nano Lett. 20, 2756–2762. https://doi.org/10.1021/acs.nanolett.0c00380.

36. Asenbauer, J., Eisenmann, T., Kuenzel, M., Kazzazi, A., Chen, Z., and Bresser, D. (2020). The success story of graphite as a lithium-ion anode material – fundamentals, remaining challenges, and recent developments including silicon (oxide) composites. Sustainable Energy Fuels 4, 5387–5416. https://doi.org/10.1039/D0SE00175A.

37. Xin, F., Zhou, H., Zong, Y., Zuba, M., Chen, Y., Chernova, N.A., Bai, J., Pei, B., Goel, A., Rana, J., et al. (2021). What is the role of Nb in nickel-rich layered oxide cathodes for lithium-ion batteries? ACS Energy Lett. 1377–1382. https://doi.org/10.1021/acsenergylett.1c00190.